Contents lists available at ScienceDirect

European Journal of Medicinal Chemistry Reports

Synthesis, anticancer activities and experimental-theoretical DNA interaction studies of 2-amino-4-phenyl-4H-benzo[h]chromene-3-carbonitrile

Taniris Cafiero Braga [a], Marina Magalhães Silva [b], Eduarda O.O. Nascimento [b], Edjan Carlos Dantas da Silva [b], Yuri de Freitas Rego [a], Mullicka Mandal [c], Zaqueu Alves de Souza [a], Ana Lúcia Tasca Góis Ruiz [d], João Ernesto de Carvalho [d], Felipe Terra Martins [e], Isis Martins Figueiredo [b], Thiago Mendonça de Aquino [b], Cleiton Moreira da Silva [a], Bhagirath Mandal [c], Goutam Brahmachari [c,**], Josué Carinhanha Caldas Santos [b,***], Ângelo de Fátima [a,*]

[a] Department of Chemistry, Universidade Federal de Minas Gerais, Belo Horizonte, MG, Brazil
[b] Institute of Chemistry and Biotechnology, Universidade Federal de Alagoas, Maceió, AL, Brazil
[c] Department of Chemistry, Visva-Bharati (a Central University), Santiniketan, 731 235, West Bengal, India
[d] Faculdade de Ciências Farmacêuticas, Universidade Estadual de Campinas, Paulínia, SP, Brazil
[e] Instituto de Química, Universidade Federal de Goiás, Goiânia, GO, Brazil

ARTICLE INFO

ABSTRACT

Twenty chromenes were synthesized with good to excellent yields (70–96%). From the series of chromenes herein tested, compounds 14, 12, 15, 16, 17, 18, and 20 were the most potent throughout the cancer human cell lines tested. In general, the *para*-position electron-withdrawing substituents on the phenyl ring are favored towards potency and selectivity for cancer cells. Biophysical studies were performed with eight chromene derivatives (13-20) and ctDNA to evaluate possible biological targets. The molecular fluorescence verified that compound 16 presented a higher binding constant (K_b) with the ctDNA, agreeing with *in vitro* biological results and that evaluated chromenes derivatives interact preferentially *via* intercalation. Finally, an inverse linear correlation ($\log K_b$ *vs.* GI_{50}) was observed for six human carcinogenic cell lines; hence, the mechanism of action of these compounds may be related to DNA interaction.

1. Introduction

Chromenes are a widespread class of oxy-containing bicyclic heterocycles, yielded by the fusion of a benzene ring with pyran (Fig. 1) [1]. These compounds are fairly ubiquitous in nature, being found in bacteria [2], fungi [2,3], plants [1,4] and animals [5]. Chromene is an important moiety in medicinal chemistry, as its derivatives exhibit a myriad of physiological activities, among them antimicrobial [6,7], antihypertensive [3], anti-coagulant [8], β-secretase inhibition [9], antitrypanosomal [10], antidyslipidemic [11], anti-HIV [12], anti-depressant [13] and anti-neoplastic [14,15]. Among these biological properties, the anticancer is one of the most promising for this class of substances. For instance, chromene **MX58151** (Fig. 1) was active for treating drug-resistant cancers [16]. Chromene **EPC2407** (Fig. 1), also known as crolibulin, is currently in phase I/II clinical trials as a vascular disrupting anti-cancer drug to treat advanced solid tumors [17,18]. Another notable example of chromene that has emerged as anticancer agents is the LY290181 (Fig. 1) (herein designed by the number **18**; Fig. 1). LY290191 is a potent antiproliferative agent for a variety of cancer cell lines which exert its effects by inhibiting the mitosis and microtubules [18,19].

Cancer is a disease in which the growth control is lost in one or more cells, leading either to a solid mass of cells known as a tumor or to non-
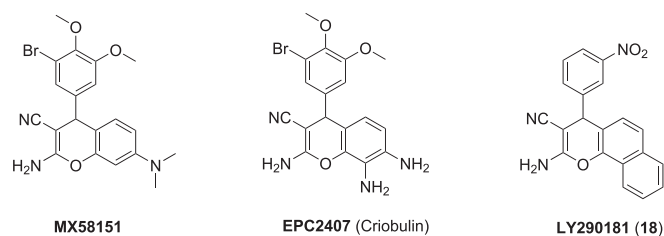
Fig. 1. Chemical structures of potential chemotherapeutic chromenes **MX58151**, **EPC2407** (also named crolibulin), and LY290191 (herein designed by the number **18**).

solid cancer such as blood or bone marrow-related cancer [20,21]. It is one of the principal causes of death throughout the world, in which the main treatments involve surgery, chemotherapy, and/or radiotherapy [20,21]. However, despite all drugs available to treat cancer, more than 18 million new cases appear yearly throughout the globe, and 10 million will die from it [22]. It is known that substances capable of DNA intercalation can act as anti-cancer agents [23–25], such as the drug doxorubicin [26]. Intercalators and minor groove binders, like distamycin, also have antiproliferative capability by inhibiting DNA-transcription factors binding [27]. It has been shown that benzothiazolyl-benz-α--chromene acts as a DNA intercalation agent [28], and 3,4-dihydropyrano [c]chromene as a non-intercalating groove binder [29]. Besides these reports, no systematic studies of ctDNA interactions for chromenes from series I, II, and III (Fig. 2) has been described so far.

In this study, we report the antiproliferative activity of 20 chromene derivatives (Fig. 2), being two novels 4H-benzo[h]chromene derivatives (fully characterized, including their crystallographic structures) against eight human cancerous cell lines and an immortalized keratinocyte standard cell line. In addition, we perform systematic studies of ctDNA interactions for these substances - the most potent antiproliferative ones - and the *in silico* studies for the most potent chromenes.

2. Results and discussion

2.1. Synthesis of chromene derivatives

The chromene derivatives **1**-**18** were synthesized using the protocol previously published by our research group [30] with good to excellent yields (Table 1). Spectroscopic chemical characterization data for **1**-**18** can be summarized and divided in two parts: the common 2-amino-4--phenyl-4H-pyran-3-carbonitrile core and the C–H activated compound fused ring. The common core presents in the FT-IR spectra the NH_2 stretch bands around 3380 cm^{-1} and 3320 cm^{-1}, cyano group stretch band at 2195 cm^{-1}, aromatic C–H stretching at 3090 cm^{-1}, and the pyran C–O stretching at 1100 cm^{-1}. In the ^1H NMR spectrum, the hydrogen H-4 on 4H-chromene is assigned to a singlet at 4.22 ppm and the amino group's protons to a singlet at 7.21 ppm. The nitrile yields a signal at 160

ppm in the ^{13}C NMR spectrum. When dimedone is used as C–H acid, a characteristic α,β-unsaturated ketone's C=O stretch is noted at 1670 cm^{-1} in the product's FT-IR spectrum. Condensation with 4-hydroxycoumarin yields a conjugated δ-lactone C=O stretching band at 1710 cm^{-1} in the FT-IR spectrum. Using α-naphthol as the C–H acid, no band in the carbonyl region is seen in the FT-IR spectrum.

In order to check the importance of the nitro substituent at the aromatic ring in LY290181(herein designed by the number **18**) to its antiproliferative properties, we decided to treat chromenes **15** and **18** with catalytic palladium on activated charcoal and hydrazine hydrate in refluxing ethanol, to afford the new aminophenyl chromenes **19** and **20** (Scheme 1). The chromenes **15** and **18** were easily obtained under the reaction conditions mentioned above, and they were obtained in nearly quantitative yields. The main spectral data differences between chromenes **19** and **20** and their nitro-derivatives are the lack of NO_2 stretch bands at 1550 cm^{-1} and the appearance of a band in 1325 cm^{-1} due to the aromatic bonded NH_2 group in the products' FT-IR spectra.

2.2. Single-crystal structures determination

The single-crystal X-ray diffraction technique elucidated the crystal structures of compounds **19** and **20**. The ORTEP-3 [32] representation of their experimental molecular backbones in the solid-state is shown in Fig. 3, and all information related to the collection, treatment, and refinement of their crystal structures are in Table 2. Compound **20** crystallized in the monoclinic centrosymmetric space group $P2_1/c$, loading the two enantiomers in the crystal structure as expected from their achiral synthesis. On the other hand, compound **19** was solved in the monoclinic non-centrosymmetric space group $P2_1$, with only one enantiomer in its crystal structure. Since no regioselectivity is expected in its synthesis, we believe that the solid sample of **19** is a conglomerate, *i.e.*, a physical mixture of crystals made up of either R or S enantiomers. Despite our high-quality X-ray diffraction data, the absolute structure could not be reliably determined since there is no atom heavier than oxygen in **19**.

Moreover, we have chosen the R enantiomer to compose the elucidated crystal structure based on its Flack parameter nearest zero [0.3(10)]. Both compounds were present with just one molecule in the asymmetric unit, which are very similar regardless of the amine group position. The three fused rings formed a nearly planar core (root-mean-square deviation of its all cyclic atoms is 0.0646 Å in **19** and 0.0295 Å in **20**). The aminobenzene ring is inclined almost perpendicularly relative to the average plane of the three fused rings, with the mean plane calculated through benzene ring forming an angle of 88.24(10) in **19** and 85.65(7)° in **20** with the least-squares plane encompassing the non-hydrogen atoms of the three fused rings. The conformation on the bond connecting the aminobenzene and the three fused rings is also similar in both compounds (the dihedral angle calculated among O1, C3, C15, and C16 is −11.2(5) in **19** and -15.6(3) in **20**). In addition, triple bonds into nitrile groups were identified [1.154(6) Å in **19** and 1.142(6) in **20**].

2.3. Antiproliferative assay

In addition to the growth inhibitory concentration for 50% of cell population (GI_{50}), that measures the toxicity of a compound against a specific cell line, the selectivity index parameter (SI) allows presuming whether a sample would affect normal proliferative tissues in similar way as tumor tissue. Furthermore, SI is an organ-specific toxic parameter and does not express other physiological interactions in living organisms [33]. Considering the I- (**1**-**6**), II- (**7**-**12**), and III- (**13**-**20**) series of chromenes and the average cytostatic effect expressed by mean $logGI_{50}$, the III-series afforded more active compounds (**13**-**16**, **18**, **20**) than I- (**2**-**3**) and II-series (**12**). Furthermore, the most active compounds in III-series shown lower selective index (SI < 2). This evidence suggested that the coumaryl (II-series) or naphthalene (III-series) cycles reduced or
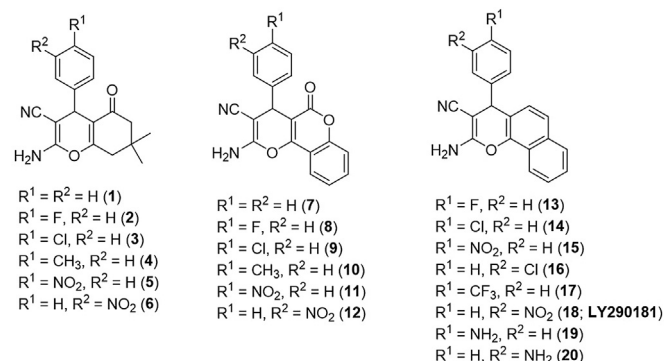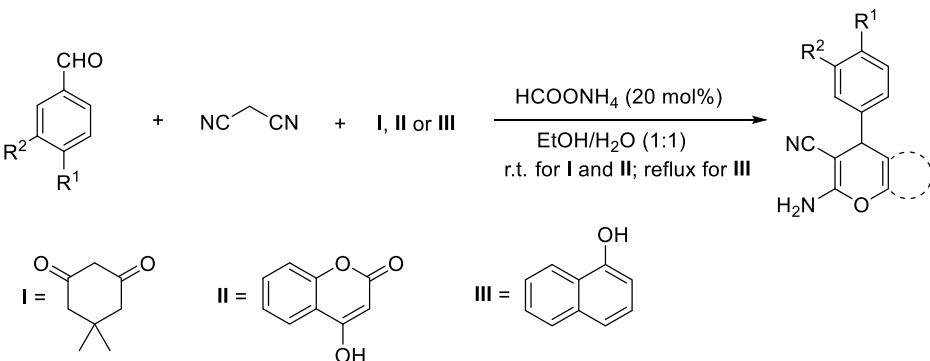
Fig. 2. Chemical structures of chromene derivatives studied in this work.

$R^1 = R^2 = H$ (**1**)
$R^1 = F, R^2 = H$ (**2**)
$R^1 = Cl, R^2 = H$ (**3**)
$R^1 = CH_3, R^2 = H$ (**4**)
$R^1 = NO_2, R^2 = H$ (**5**)
$R^1 = H, R^2 = NO_2$ (**6**)

$R^1 = R^2 = H$ (**7**)
$R^1 = F, R^2 = H$ (**8**)
$R^1 = Cl, R^2 = H$ (**9**)
$R^1 = CH_3, R^2 = H$ (**10**)
$R^1 = NO_2, R^2 = H$ (**11**)
$R^1 = H, R^2 = NO_2$ (**12**)

$R^1 = F, R^2 = H$ (**13**)
$R^1 = Cl, R^2 = H$ (**14**)
$R^1 = NO_2, R^2 = H$ (**15**)
$R^1 = H, R^2 = Cl$ (**16**)
$R^1 = CF_3, R^2 = H$ (**17**)
$R^1 = H, R^2 = NO_2$ (**18**; **LY290181**)
$R^1 = NH_2, R^2 = H$ (**19**)
$R^1 = H, R^2 = NH_2$ (**20**)

Table 1
Reactions conditions[a], reagents, and yields values obtained in the synthesis of chromenes **1**-**18**.

Chromene	R^1	R^2	C–H acid-reagent	Yield (%)	Chromene	R^1	R^2	C–H acid-reagent	Yield (%)
1[b]	H	H	I	90	**10**[b]	CH$_3$	H	II	96
2[b]	F	H	I	80	**11**[b]	NO$_2$	H	II	91
3[b]	Cl	H	I	93	**12**[b]	H	NO$_2$	II	92
4[b]	CH$_3$	H	I	81	**13**[b]	F	H	III	70
5[b]	NO$_2$	H	I	80	**14**[b]	Cl	H	III	82
6[b]	H	NO$_2$	I	87	**15**[b]	NO$_2$	H	III	87
7[b]	H	H	II	90	**16**[c]	H	Cl	III	85
8[b]	F	H	II	91	**17**[c]	CF$_3$	H	III	87
9[b]	Cl	H	II	92	**18**[c]	H	NO$_2$	III	83

^a *Reactions conditions*: aldehyde (1.0 mmol), malononitrile (1.1 mmol), HCOONH$_4$ (0.2 mmol), I/II/III (1.1 mmol), EtOH/H$_2$O 1:1 (4 mL).
^b These substances were synthesized as per the reported methodology published elsewhere by our research group [30].
^c These substances were synthesized by our methodology, and their data is in accordance with the literature [31].
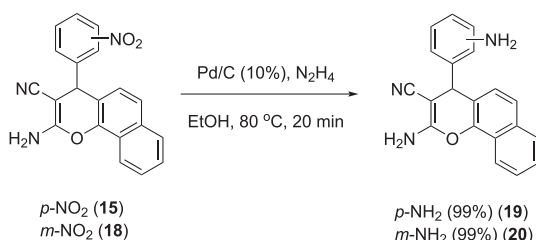
Scheme 1. Chemoselective hydrogenation reaction of the nitro group for preparation of chromenes **19** and **20**.

improved, respectively, the cytostatic effect observed for **I**-series while the ligands R^1 and R^2 could modulate the selectivity (Table 3).

Compounds in **I**-series (**1**-**6**) showed an interesting selective inhibition of ovarian tumor cells (NCI-ADR/RES and OVCAR-03). Compound **1** (R^1 = R^2 = H) showed potent cytostatic effect (GI$_{50}$ < 0.8 μM) for both

ovarian tumor cell lines in a highly selective manner (SI > 800). Moreover, non-electrophilic R^1 substituents such as H (compounds **1** and **6**) and CH$_3$ (compound **4**) resulted in better activity against multi-drug resistant NCI-ADR/RES cells. Electrophilic substituents (R^1 = F, **2** and R^1 = Cl, **3**) at *para* position did not affect the activity against OVCAR-03 cells although reduced the effect against multi-drug resistant ovarian tumor cells (NCI-ADR/RES). Additionally, compound **3** showed promising antiproliferative effect against non-small cell carcinoma of lung (NCI–H460), being the series' most active compound against this cell line (Table 3).

Almost all **II**-series compounds were inactive considering the mean effect against all tested tumor cell lines except by compound **12** suggesting that the coumaryl substituent did not favor the biological effect. Considering R^1 and R^2 substituents, the best choice was the nitro group at *meta* position (compound **12**) for antiproliferative activity against all tumor cell lines. Furthermore, compounds **8**, **11** and **12** were more active against OVCAR-03 cell line than against NCI-ADR/RES cells while compound **10** showed an inverse preference (GI$_{50}$ NCI-ADR/RES < GI$_{50}$
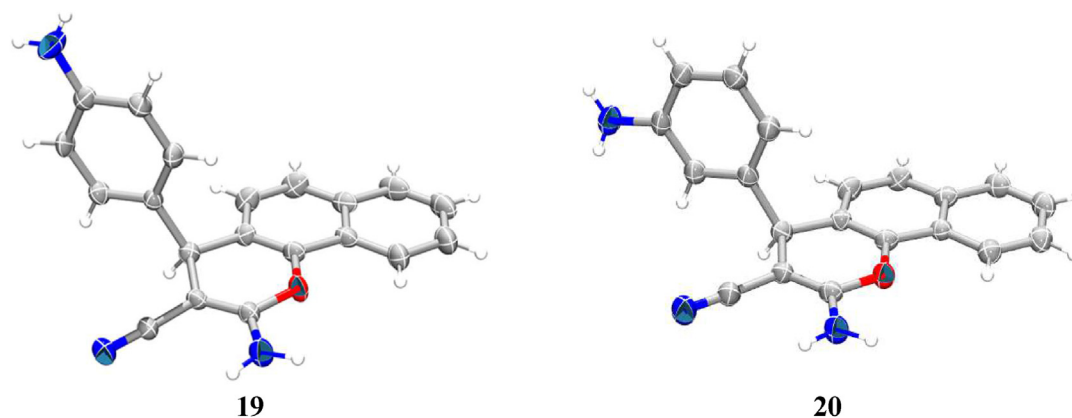

Fig. 3. The asymmetric unit of chromenes **19** and **20** is elucidated in this study. Non-hydrogen atoms are represented as 30% probability ellipsoids following a random labeling scheme (shown once), while hydrogens are shown as arbitrary radius spheres.

Table 2
Crystal data and refinement parameters of compounds reported in this study.

Parameters		19	20
structural formula		$C_{20}H_{15}N_3O$	$C_{20}H_{15}N_3O$
fw (g/mol)		313.35	313.35
cryst syst		monoclinic	monoclinic
space group		*P21*	*P21/c*
Z/Z'		2/1	4/1
T (K)		296(2)	296(2)
unit cell dimensions	*a* (Å)	9.928(3)	12.901(4)
	b (Å)	5.5895(17)	10.512(3)
	c (Å)	14.094(5)	12.502(3)
	β (°)	93.10(2)	112.219(6)
V (Å^3)		781.0(5)	1569.7(8)
calculated density (Mg/m^3)		1.332	1.326
absorption coefficient μ (mm^{-1})		0.085	0.084
θ range for data collection (°)		2.895 to 25.414	2.581 to 25.419
index ranges	*h*	−11 to 11	−15 to 12
	k	−5 to 6	−12 to 12
	l	−8 to 17	−6 to 15
data collected		3261	6213
unique reflections		2277	2852
unique reflections with *I* > 2σ(*I*)		1809	1639
symmetry factor (Rint)		0.0167	0.0354
completeness to *θ* max (%)		97.4	98.5
F (000)		328	656
parameters refined		217	217
goodness-of-fit on *F2*		1.102	1.017
final *R* factors for *I* > 2σ(*I*)		R1 = 0.0433 wR2 = 0.0971	R1 = 0.0538 wR2 = 0.1286
R factors for all data		R1 = 0.0598 wR2 = 0.1101	R1 = 0.1006 wR2 = 0.1546
largest diff. peak/hole (e/ Å3)		0.134 and −0.191	0.190 and −0.203
CCDC deposit number		1978913	1978914

OVCAR-03), following a similar rationalization observed for **I**-series compounds (Table 3).

The most promising compound series, **III**, had 6 active compounds out of 8. Presenting a naphthalene substituent, these compounds showed cytostatic effect against both tumor and non-tumor human cell lines. These effects were expressed as selective indexes (SI) lower than 2 for almost all tumor cell lines for some of the active compounds, such as compounds **13**, **16**, **17** and **20**. (Table 3). The reduction of the aryl's nitro group, **15** and **18**, to amino, **19** and **20**, lead to a lower antiproliferative activity overall. Hence, the most promising compound tested was **15** (Table 3), inhibiting K562 (chronic myelogenous leukemia), U251 (glioblastoma), 786-0 (kidney, adenocarcinoma), NCI–H460 (non-small cell carcinoma), NCI/ADR-RES (multidrug resistant ovarian adenocarcinoma), and PC-3 (prostate, adenocarcinoma) with GI$_{50}$ lower than 10 μM and SI higher than 30 times.

2.4. Biophysical studies of ctDNA interaction with chromene derivatives

2.4.1. Evaluation of the interaction chromene-ctDNA by molecular fluorescence

Biophysical studies of chromenes derivatives interaction with ctDNA were performed to evaluate these compounds' possible action mechanisms. Thus, **13-20** were selected, highlighting biological activity against the human carcinogenic cell lines (Table 3). The compound 16 was one of the most active; thus, it was used as a model to present the results. Since chromene derivatives have intrinsic fluorescence [34], a spectrofluorimetric titration [35] was carried out to study the interaction process of these compounds with ctDNA. In general, for most of the evaluated compounds (**13-16**), when adding increasing increments of ctDNA to the system, there was a gradual decrease in the analytical signal

(fluorescence intensity), indicating that interaction between the evaluated compounds and the macromolecule is occurring [36], with the formation of a supramolecular complex. However, for the reduced derivatives (**19** and **20**), the addition of ctDNA led to an increase in the analytical signal, possibly due to the microenvironment in which these molecules are inserted in the DNA, which must have less polarity, being more hydrophobic concerning the original condition of the molecule in an aqueous medium [37]. Fig. 4A shows the spectral profile obtained for compound **16**.

The reduction of the fluorescence intensity (analytical signal) in the presence of a quencher compound (in this case, the ctDNA) is called the quenching process [38], described mathematically by the Stern-Volmer equation:

$$\frac{F_0}{F} = 1 + K_{SV}[Q] \tag{1}$$

F$_0$ and F represent the fluorescence intensities in the absence and presence of the macromolecule, respectively; [Q] represents the concentration of ctDNA (quencher molecule), and K$_{SV}$ is the Stern-Volmer constant. It is noteworthy that the quenching mechanism is only considered when there is a reduction in fluorescence [39] since, in many cases, the addition of DNA can increase the analytical signal, as observed for compounds **19** and **20**.

Based on the variation in fluorescence intensity in the presence of ctDNA, the DNA-chromenes interaction constant (*K*$_b$) was calculated, aiming to evaluate the strength of this interaction process, as well as the number of binding sites (*n*) [40]:

$$\log\left[\frac{(F_0 - F)}{F}\right] = \log K_b + n\log[\text{ctDNA}] \tag{2}$$

Fig. 4B and C shows the curves obtained for the chromene derivative **16** by linearizing equations (1) and (2), respectively, while Table 4 presents the results obtained for this assessment.

The K$_{SV}$ values ranged from 3.02 to 6.90 × 10^3 M^{-1}, indicating a decrease in analytical signal in the presence of the quencher molecule (ctDNA) (Table 4). Several mechanisms are related to the quenching process; the main ones are dynamic (collisional) or static quenching, but in some situations, both mechanisms occur simultaneously [41]. Thus, to assess the type of preferential quenching in the interaction process, the K$_{SV}$ values at different temperatures (23, 30, and 37 °C, in this case) were evaluated. When the K$_{SV}$ values increase due to the increase in temperature, it indicates dynamic quenching since, at higher temperatures, there is a more significant diffusion coefficient, and consequently, a greater number of collisions between the fluorescent ligand and the quencher (DNA). On the other hand, when K$_{SV}$ values decrease with increasing temperature, it characterizes static quenching, considering that process destabilizes the DNA-ligand complex [42]. From the results obtained (Table 4), with increasing temperature, the values of the Stern-Volmer constants decrease, indicating that the dominant quenching mechanism is static [43], with the formation of a supramolecular complex non-fluorescent.

The *K*$_b$ values were obtained from 0.010 to 20.2 × 10^4 M^{-1}, demonstrating the magnitude of the binding of the chromene-ctDNA complex, being considered of high affinity for the compounds **13** and **16** (*K*$_b$ ≥ 10^5), a medium affinity for the compounds **14**, **15**, **17**, and **18** (*K*$_b$ ≥ 10^3) and low affinity for **19** and **20** [44]. Besides, it appears that the *n* values were close to the unit indicating a stoichiometric ratio 1:1 (ctDNA:chromene). The **16** chromene derivative showed a high interaction constant with the ctDNA, which may be related to the presence of a chlorine substituent. According to Benner et al. [45] and Krautwald et al. [46], the chlorine atom may replace the methyl group (bioisosteric) without changing the steric demand of a compound since chloro, and methyl groups are univalent and have van der Waals radii that differ by about 15%. Besides, the chloro-substituent associated with the annellation process (Table 1) may increase the binding affinity of the ligand for

Table 3
The concentration of the chromenes (GI$_{50}$; μM)[a] that elicits cells growth inhibition by 50% and the most relevant selective index (SI)[b] values.

Compound	U251		MCF-7		NCI/ADR-RES		786-0		NCI–H460		PC-3		OVCAR-03		K-562		Mean logGI$_{50}$[d]	HaCaT
	GI$_{50}$[a]	SI[b]	GI$_{50}$[a]	SI[b]	GI$_{50}$[a]	SI[b]	GI$_{50}$[a]	SI[b]	GI$_{50}$[a]	SI[b]	GI$_{50}$[a]	SI[b]	GI$_{50}$[a]	SI[b]	GI$_{50}$[a]	SI[b]		GI$_{50}$[a]
1	154.7	>4	>650	*	<0.8	>812	225.8	>3	25.5	>25	433.5	*	<0.8	>812	467.8	*	>1.7 I	>650
2	87.5	*	79.8	*	1.3	64	91.0	*	126.6	*	76.3	*	<0.8	>104	43.6	2	1.4 W	83.3
3	93.8	*	77.8	*	4.3	*	177.1	*	0.4	2	>650	*	<0.8	*	4.6	*	>1.2 W	0.8
4	181.4	>4	399.8	>2	0.7	>102	197.3	>3	255.1	>3	298.2	>2	101.9	6	0.9	>722	1.7 I	>650
5	79.9	*	77.5	*	76.7	*	75.2	*	79.6	*	75.8	*	14.4	5	33.3	2	1.8 I	72.5
6	76.1	*	75.0	*	<0.8	*	72.0	*	66.3	*	161.9	*	1.4	58	>650	*	>1.6 I	81.7
7	>650	*	>650	*	111.0	>6	>650	*	>650	*	>650	*	>650	*	>650	*	>2.7 I	>650
8	333.1	>2	>650	*	1.2	>542	200.5	*	1.2	>542	206.5	>3	<0.8	>813	621.4	*	>1.6 I	>650
9	167.2	>4	>650	*	>650	*	91.4	>7	>650	*	>650	*	>650	*	>650	*	>2.6 I	>650
10	372.3	*	276.4	*	10.5	18	73.4	3	>650	*	450.3	*	84.2	2	>650	*	>2.3 I	185.3
11	212.4	>3	550	*	0.8	>812	191.6	>3	>650	*	>650	*	1.1	591	>650	*	>2.0 I	>650
12	17.7	*	5.4	*	1.2	7	8.8	*	3.8	2	8.2	*	<0.8	>10	24.0	*	<0.7 M	7.9
13	0.8	9	>650	*	2.0	3	2.3	3	6.1	*	46.4	*	27.4	*	>650	*	>1.3 W	6.9
14	2.1	2	33.0	*	2.5	*	4.3	*	4.9	*	26.7	*	18.0	*	3.5	*	0.8 M	3.2
15	1.4	>464	41.3	>16	3.2	>203	1.9	>342	7.8	>83	4.1	>159	21.4	>30	0.2	>3250	0.6 M	>650
16	5.3	*	18.8	*	3.5	*	4.8	*	19.8	*	8.8	*	7.4	*	2.8	*	0.8 M	3.0
17	51.3	*	>650	*	8.8	*	8.0	*	58.3	*	30.3	*	11.4	*	11.7	*	>1.5 I	8.0
18	1.0	4	>650	*	1.2	3	1.3	3	13.0	*	5.2	*	14.1	*	0.5	7	>0.7 M	3.6
19	14.0	>46	>650	*	>650	*	50.0	>13	>650	*	6.8	>96	>650	*	>650	*	>2.2 I	>650
20	3.1	*	19.7	*	17.1	*	31.4	*	27.4	*	<0.8	*	22.3	*	0.3	3	0.8 M	0.9
DOX[c]	<0.05	*	<0.05	*	0.055	*	0.055	*	0.055	*	0.18	*	<0.05	*	0.28	*	<-1.1 P	<0.05

Human tumor cell lines: U251, glioblastoma; MCF7, breast, adenocarcinoma; NCI-ADR/RES, ovary, multidrug-resistant adenocarcinoma; 786-0, kidney, adenocarcinoma; NCI–H460, lung, non-small cell carcinoma; PC-3, prostate, adenocarcinoma; OVCAR-3, ovary, adenocarcinoma; K-562, chronic myelogenous leukemia; Human non-tumor cell line: HaCaT, immortalized keratinocytes.

[a] GI$_{50}$ = sample concentration (μM) required to elicit 50% of cell growth inhibition (cytostatic effect).

[b] The selectivity index was determined as the ratio of the GI$_{50}$ for HaCat to the GI$_{50}$ for the tumor cell line; only the most relevant SI values (SI ≥ 2) were presented in Table 3.

[c] DOX is the reference drug doxorubicin; (*) SI < 2.

[d] Mean log GI$_{50}$ = arithmetic mean of the GI$_{50}$ values expressed as logarithm; NCI's criteria: I, inactive (mean log GI$_{50}$ > 1.50); W, weak activity (1.50 ≥ mean log GI$_{50}$ > 1.10); M, moderate activity (1.10 ≥ mean log GI$_{50}$ > 0); P, potent activity (mean log GI50 <0). Data are means of a representative experiment done in triplicate.
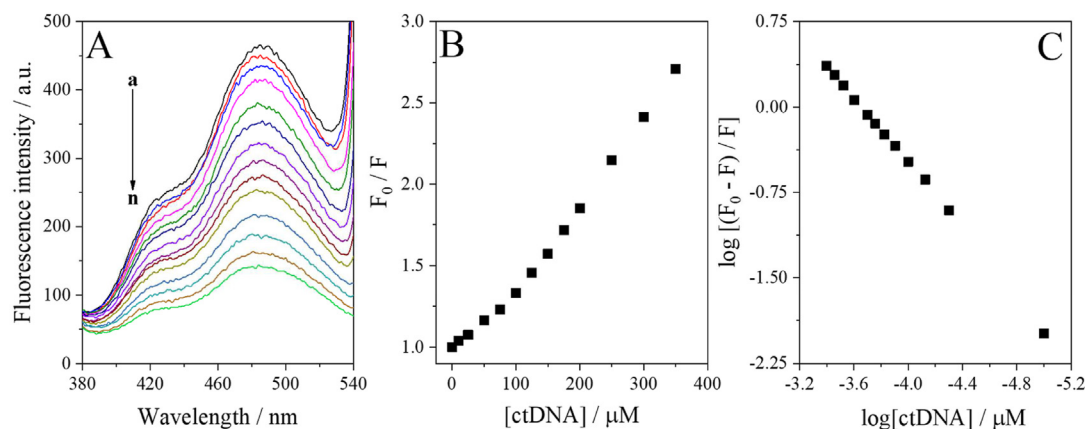
Fig. 4. Results were obtained for the evaluation of the DNA-chromene interaction process by molecular fluorescence. (A) The spectral profile of compound **16** (10 μM) with the addition of increasing increments of ctDNA (10, 25, 50, 75, 100, 125, 150, 175, 200, 250, 300, 350, 400 μM, curves a-n, respectively); (B) Stern-Volmer plot for compound **16** (evaluation of quenching process); (C) Double logarithmic curve for calculating the binding constant (K_b).

Table 4
Interaction parameters of calf thymus DNA (ctDNA) with chromenes derivatives at 23, 30, and 37 °C.

Chromene	Temperature (°C)	Stern-Volmer constant		Binding parameters			Thermodynamic parameters		
		K_{SV} (10^3 M^{-1})	r	K_b (10^4 M^{-1})	n	r	ΔG (kJ mol^{-1})	ΔH (kJ mol^{-1})	ΔS (J K^{-1} mol^{-1})
13	23	7.48 ± 0.38	0.9861	16.4 ± 0.05	1.40 ± 0.05	0.9954	−89.35	−59.61	−100.5
	30	6.90 ± 0.32	0.9893	13.8 ± 0.07	1.37 ± 0.04	0.9961	−90.06		
	37	6.13 ± 0.34	0.9868	5.46 ± 0.03	1.29 ± 0.04	0.9958	−90.76		
14	23	3.90 ± 0.46	0.9480	7.49 ± 0.08	1.41 ± 0.15	0.9572	−139.7	−83.92	−188.5
	30	3.70 ± 0.33	0.9620	6.43 ± 0.04	1.38 ± 0.08	0.9879	−141.0		
	37	3.54 ± 0.26	0.9763	1.59 ± 0.03	1.14 ± 0.09	0.9797	−142.3		
15	23	3.23 ± 0.11	0.9948	1.57 ± 0.09	1.21 ± 0.04	0.9956	−166.5	−95.38	−240.1
	30	3.02 ± 0.10	0.9934	1.23 ± 0.05	1.18 ± 0.04	0.9961	−168.1		
	37	2.65 ± 0.10	0.9949	0.27 ± 0.01	0.99 ± 0.05	0.9906	−169.8		
16	23	5.68 ± 0.20	0.9928	21.7 ± 0.06	1.46 ± 0.05	0.9924	−33.75	−32.09	−5.62
	30	5.41 ± 0.25	0.9888	20.2 ± 0.08	1.45 ± 0.02	0.9994	−33.79		
	37	5.02 ± 0.27	0.9898	12.0 ± 0.07	1.38 ± 0.02	0.9989	−33.83		
17	23	3.58 ± 0.31	0.9712	4.68 ± 0.02	1.33 ± 0.06	0.9957	−102.7	−64.47	−129.2
	30	3.18 ± 0.12	0.9957	1.92 ± 0.07	1.19 ± 0.10	0.9749	−103.6		
	37	2.74 ± 0.15	0.9910	1.44 ± 0.05	1.17 ± 0.09	0.9792	−104.5		
18	23	4.01 ± 0.12	0.9948	3.31 ± 0.04	0.99 ± 0.04	0.9911	−167.5	−93.47	−250.9
	30	3.93 ± 0.16	0.9912	1.52 ± 0.02	0.81 ± 0.04	0.9911	−169.3		
	37	3.84 ± 0.17	0.9910	0.94 ± 0.03	0.77 ± 0.07	0.9670	−171.0		
19	23	-	-	0.062 ± 0.003	0.95 ± 0.09	0.9793	−16.04	−37.61	−73.1
	30	-	-	0.058 ± 0.005	0.88 ± 0.05	0.9877	−15.46		
	37	-	-	0.028 ± 0.007	0.83 ± 0.18	0.9145	−14.87		
20	23	-	-	0.019 ± 0.004	0.78 ± 0.04	0.9868	−8.11	−38.41	−102.7
	30	-	-	0.016 ± 0.005	0.85 ± 0.05	0.9838	−7.29		
	37	-	-	0.010 ± 0.006	0.89 ± 0.02	0.9818	−6.47		

the macromolecule. Finally, this work is an exploratory study using a healthy DNA model. Therefore, for compounds with greater selectivity for tumor lines such as **15** (Table 3), there was a reduction in the K_b. Thus, not only structural aspects can be considered, but also the macromolecule model used in the investigation to justify the variations in K_b values.

Table S1 (supplementary material) presents several studies that evaluate the interaction of chromene derivatives with ctDNA by molecular fluorescence [34,37,47], which show different spectroscopic characteristics in the presence of DNA; that is, they can increase or decrease the fluorescence intensity when interacts with the macromolecule. In addition, it was observed that K_b values are similar to those found in our study, ranging from 10^3 to 10^5 M^{-1}; and, besides, these compounds interact preferentially by intercalation mode (discussed in a posteriori topic).

The thermodynamic parameters involved in the interaction of ligands with DNA were determined. Hydrogen bonds, van der Waals forces, hydrophobic and electrostatic interactions are the four main non-covalent interactions, which play an essential role in the nucleic acid

and ligand interaction [48]. The formation of complexes between ligands and DNA can be studied at different temperatures, enabling the determination of various thermodynamic parameters such as variation in enthalpy (ΔH) and entropy (ΔS) through the application of the Van't Hoff equation [49]:

$$\ln(K_b) = -\frac{\Delta H}{R} \times \left[\frac{1}{T}\right] + \frac{\Delta S}{R} \quad (3)$$

K_b represents the binding constant, T is the temperature in Kelvin (K), and R the ideal gas constant (8.314472 J K^{-1} mol^{-1}). The Gibbs free energy value can be calculated as a function of the values of ΔH and ΔS:

$$\Delta G = \Delta H - T\Delta S \quad (4)$$

The values of ΔH and ΔS for all compounds were both negative (Table 4), indicating that hydrogen bonds and van der Waals interactions are the preferred ones in the interaction process [50]. Besides, it is observed that the ΔG values are negative, demonstrating the spontaneity of the interaction process.

2.4.2. UV–vis spectroscopy studies

UV–Vis spectroscopy is a technique widely used in studies of DNA-ligand interaction because spectral modifications provide information about the formation of a supramolecular complex formed between the evaluated compound and the macromolecule [51]. Thus, the interaction of ligands with ctDNA was assessed, and after the ctDNA addition to the system with the chromene derivative, an increase in the absorbance signal concerning the free compound (Fig. S1, supplementary material), characterizing a hyperchromic effect. It is worth mentioning that when the ligand interacts with the ctDNA, forming a complex, changes in the absorbance values and the position of the band can occur due to electronic transitions $n \rightarrow \pi^*$ and $\pi \rightarrow \pi^*$ of the ligands and $\pi \rightarrow \pi^*$ of the macromolecule. Thus, to assess whether there is the formation of a supramolecular complex between the chromene derivative and the macromolecule, the absorbance values of the chromene-ctDNA mixture ($A_{complex}$) must be different from the sum of the absorbance values of the free chromene and ctDNA ($A_{ligand} + A_{DNA}$), that is, $\Delta A = A_{complex} - (A_{ligand} + A_{DNA})$ is different from zero ($\Delta A \neq 0$) [52].

The ΔA values showed positive variation for all compounds (Table S2), indicating that there is an interaction between the ligands evaluated and the macromolecule, with the formation of a supramolecular complex in the ground state, characterizing the static quenching process [52,53], and confirming the mechanism proposed by molecular fluorescence studies. Besides, the difference between the complex ($A_{ligand-DNA}$) and the free ctDNA was not overlapped on the spectrum of the pure compound (Fig. S1), confirming that there was a change in the ground state due to the formation of the chromene derivative complex with nucleic acid [39].

2.4.3. Preferential interaction mode of DNA-chromene derivatives interaction

The binding mode of chromene derivatives with ctDNA was assessed, initially using KI quenching assay, to verify the degree of protection of the ligands [53]. Rehman et al. reported that negatively charged iodide ions could promote dynamic quenching in fluorescent compounds. However, the ligand must be accessible to this quencher species [53]. Therefore, Stern-Volmer constants values are compared in the presence and absence of the ctDNA. In general, the intercalation of ligands in the double helix of the nucleic acid prevents the anionic inhibitor from having access to the ligands, leading to a decrease in the K_{SV} value in the presence of DNA. In contrast, when the ligands preferentially interact via groove or electrostatic mode, the ligands are more accessible to the surrounding iodide ion, and the K_{SV} values in the presence of DNA tend to be higher since there is a more amount of the free ligand in solution [54]. Fig. 5A shows the results obtained for this assay. The K_{SV} values in the presence of DNA were systematically lower than in the absence of the macromolecule, indicating that the chromene derivatives are protected

by the double helix of the nucleic acid, making it difficult for iodide anion to access [55]. These results suggest that the evaluated compounds can interact preferentially by intercalation.

A competition study was carried out with methylene blue (MB), a phenothiazinium dye that binds to DNA via intercalation [56], to confirm the KI assay results. When free, MB shows significant quantum yield (high fluorescence intensity), but when bound to DNA, its fluorescence decreases considerably. In this sense, the presence of a small molecule with the same DNA binding mode in the system can lead to the displacement of the intercalated MB, consequently leading to an increase in fluorescence intensity, since part of the MB would be in the free form, that is, not intercalated between nitrogenous bases [53]. In this study, synchronized fluorescence was used, a robust analytical method, efficient to detect the interaction of ligands with macromolecules due to the achievement of narrow and well-resolved emission spectra [57]. Thus, an $\Delta \lambda = 40$ nm ($\lambda_{em} - \lambda_{ex}$) was used to eliminate the spectral interference resulting from the emission of the chromene derivatives and consequently evaluate the profile of the MB-ctDNA spectrum in the presence of increasing amounts of the evaluated ligands. Thus, when the chromene derivative 16 was added to the MB-ctDNA system, a gradual increase in the analytical signal (Fig. 5B) was observed, ranging from 24 to 54% (excess of 25 times, Fig. 5C). Furthermore, the displacement of the MB from ctDNA leads to a hyperchromic and bathochromic effect (red-shift), respectively, indicating that chromenes derivatives are competing for the same dye-binding site, therefore, suggesting that these compounds can interact with nucleic acid preferentially via intercalation [58].

Finally, these results reinforce the data obtained in the potassium iodide assay and agree with different studies [34,37,47], that evaluated the interaction of chromene derivatives with ctDNA by fluorescence (Table S1), and thus, indicate that the preferential interaction mode is by intercalation.

2.4.4. Correlation between binding constant and growth inhibition (GI₅₀) in elicits cells

The bioanalytical correlation analysis was performed between the values of the binding constants ($\log K_b$) of the chromene derivatives with the ctDNA (Tables 3 and 4) and the biological activity (GI$_{50}$, μM) regarding the human cancer cell lines (Fig. 6). This strategy seeks to assess whether these independent variables (K_b and GI$_{50}$) correlate and whether the possible mechanism of action may be associated with interaction with DNA. However, it is worthy of mentioning that this evaluation's objective was to establish an initial exploratory analysis of the results using the correlation between binding constant and antiproliferative activity since more effective conclusions would require a significant number of variables. The degree of association was assessed using the coefficients of linear correlation (r, Pearson coefficient). The correlation was performed only for the compounds with GI$_{50} < 650$ μM
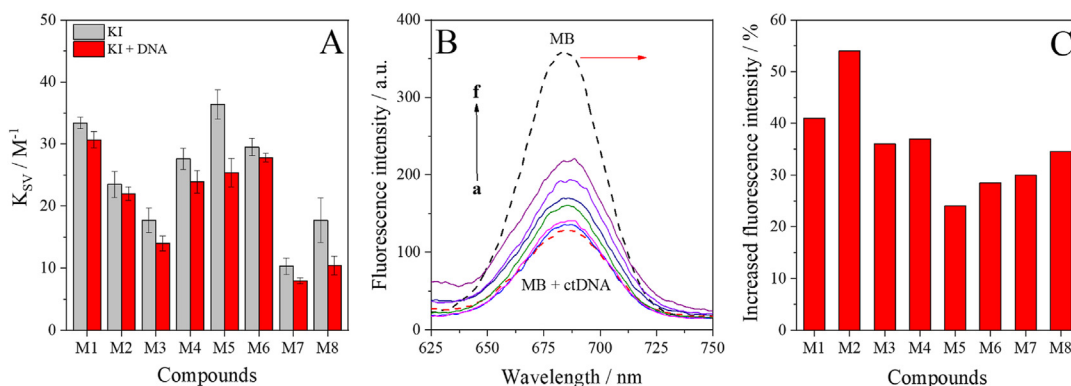

Fig. 5. Evaluation of DNA-ligand interaction mode. (A) KI quenching assay; (B) Competition with methylene blue (1.5 μM) by synchronized fluorescence of the **16** derivative (1.5, 3.75, 7.5, 15, 30, 37.5 μM, a-f curves, respectively); (C) Percentage of fluorescence increase due to the competition of the evaluated compounds with MB. (For interpretation of the references to colour in this figure legend, the reader is referred to the Web version of this article.)
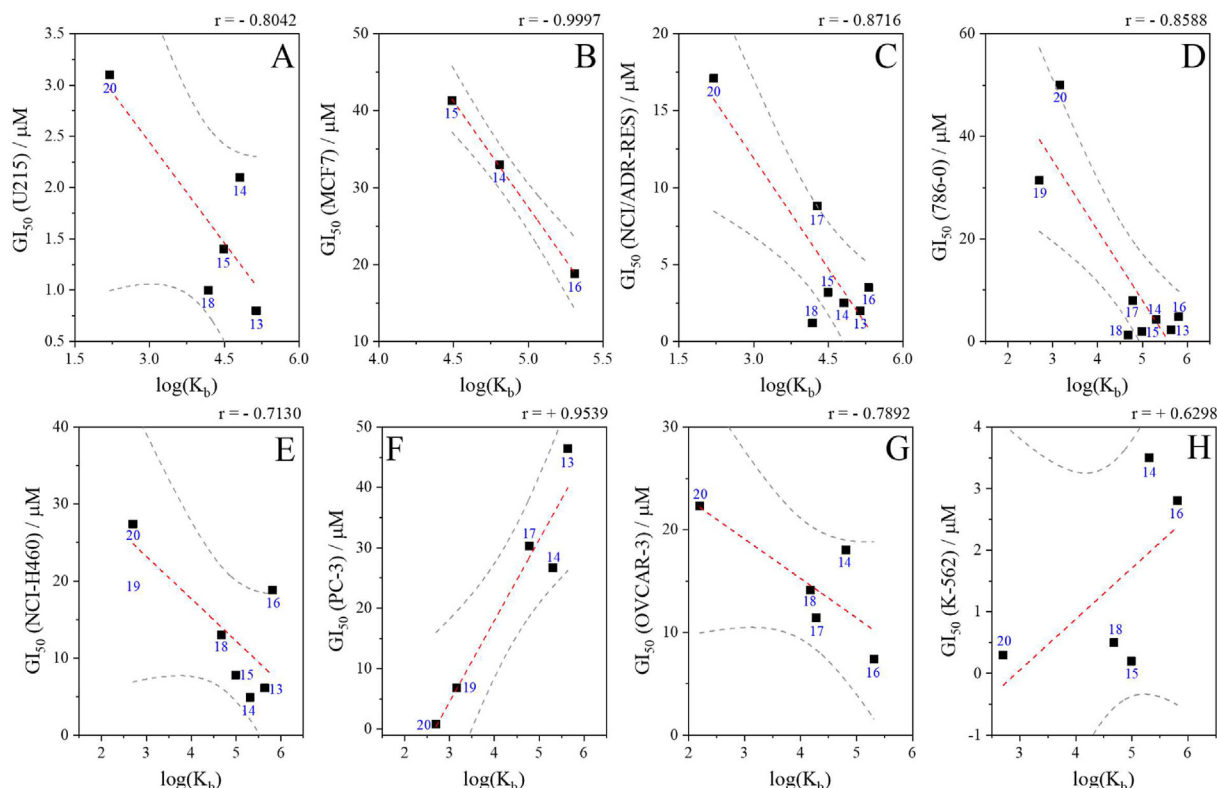
Fig. 6. Linear correlation between the values of binding constants of chromene derivatives with ctDNA (logK_b, M^{-1}) and biological activities (GI$_{50}$, μM) against different human cancer cell lines [A = glioma (U251); B = MCF7 (breast); C = NCI-ADR/RES (multiple drug-resistant ovarian cancer), D = 786-0 (renal); E = NCI–H460 (non-small lung); F = PC-3 (prostate), G = OVCAR-3 (ovarian); and H = K-562 (leukemia)]. The gray lines indicate the 95% confidence interval in each system.

values, limiting the number of points used in the mathematical modeling for each system.

In this work, it was possible to relate the antiproliferative activities with the K_b values, and in general, an inverse linear trend was obtained, that is, the higher the value of the binding constant, the lower the value of the biological activity (GI$_{50}$), and thus more active are the compounds for the cancer human cell lines evaluated. A direct linear trend was obtained only for the PC-3 (prostate) and K-562 (leukemia) human cells. However, a limitation of this type of evaluation implies using a healthy DNA model (unmutated), different from that present in tumor cells. Therefore, the variations observed between compounds **16** (high K_b, absent of selectivity) and **15** (moderate K_b, high selectivity for tumor cells) are justified considering this aspect and not just variations in molecular structure.

The values of the correlation coefficients obtained by the graph logK_b vs. GI$_{50}$ (Fig. 6) varied in the range of $-0.9997 \leq r \leq 0.9539$, with the glioma, breast, multiple drug-resistant ovarian, renal, non-small lung, and ovarian lineages presenting a linear inverse tendency (95% confidence interval). These data suggest that one of the possible mechanisms of action of these compounds is associated with interaction with DNA as the main biological target. Finally, these results corroborate studies already reported in the literature that performed correlation analysis for antiproliferative activity against human tumor cell lines for β-carboline derivatives [44], Schiff bases [59], acridines [60], and piperidines [61].

2.5. Theoretical studies of ctDNA interaction with chromene derivatives

In order to corroborate with experimental results, eight docking and MD simulations were carried out to obtain detailed information about the interactions of **13-18** derivatives with ctDNA. Molecular docking analysis revealed that all compounds interacted with the larger ctDNA groove by

non-covalent interactions, showing similar lower energy conformations (Fig. 7A). After, these conformations were chosen as the initial point for MD simulations since the DNA remains rigid during docking, and molecular dynamic provides the native structure of the DNA in a physiological medium, allowing a reorganization of the DNA bases and improving the spacing between them [61,62].

After 40 ns of simulation, all compounds intercalated between the DNA base pairs, and the most representative conformations during each simulation are shown in Fig. 7A. MD revealed modifications in the conformation, separation of some base pairs, and double helix elongation of DNA during the simulation due to the **13-18** derivatives between the DNA base pairs. These deformations in the trajectories of the DNA atoms can also be seen through the RMSD plots (Fig. 7B). In the first 5 ns of simulation, it is possible to observe a more significant deviation of the DNA atoms caused by the change in the mode of interaction of the compounds. After, the RMSD values decrease and remain stable until the end of the simulation, demonstrating the stability of the interactions for all derivatives by intercalation mode. The means of these deviations did not exceed 0.25 nm, evidencing that the DNA did not denature during the simulations. The results demonstrated a strong relation between fluorescence quenching assay and theoretical results.

Among the compounds analyzed, derivative **16** showed lower RMSD values during MD simulation, evidencing higher stability of this intercalation mode (Fig. 7C). This result may explain that this compound presented higher affinity in the biophysical assays, suggesting that DNA may be the main biological target for cytotoxicity against cancer cell lines. Finally, all the ligand-DNA complexes were stabilized by intermolecular hydrogen bond and van der Waals interactions, corroborating with negative values of the thermodynamic parameter ΔS and ΔH calculated by molecular fluorescence (Table 4) [52,53].
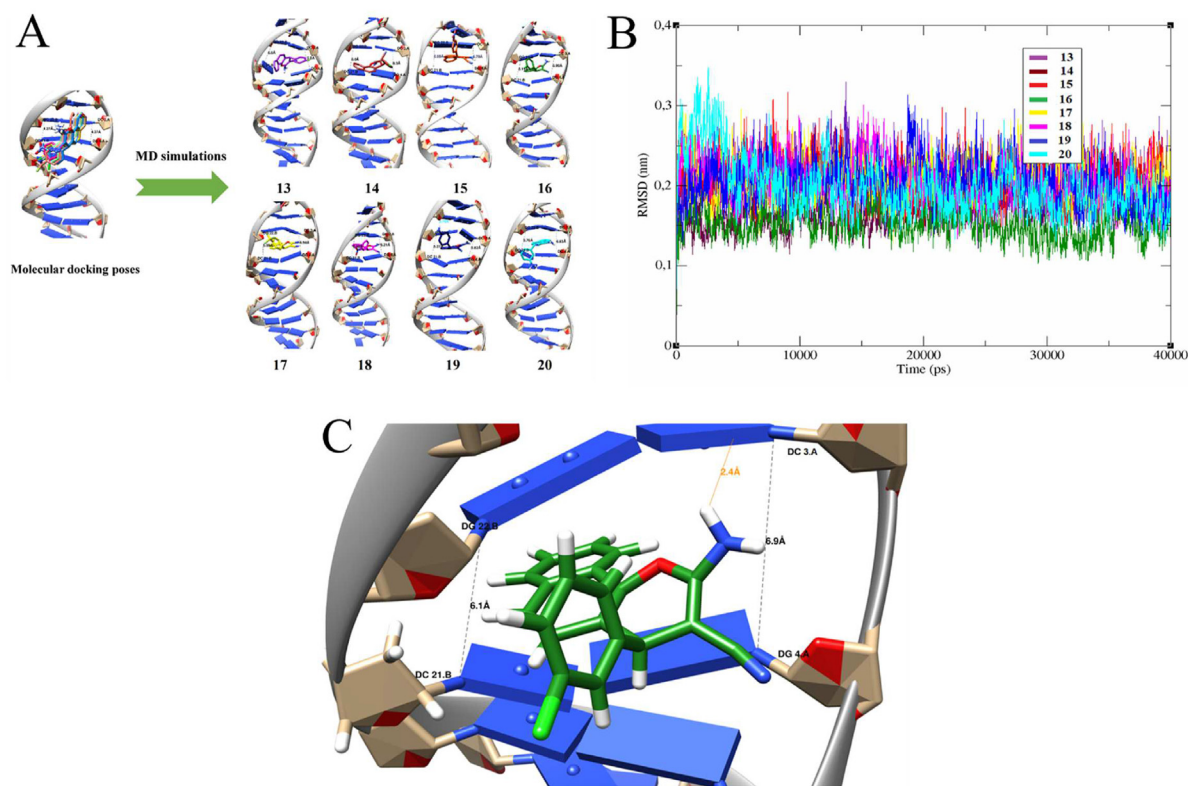
Fig. 7. (A) Molecular docking poses (clustering) of the compounds **13-20** interacting with the ctDNA larger groove after docking procedure, and representative frames of each compound after molecular dynamics simulations, showing that all compounds intercalate into the DNA bases; (B) Root mean square deviation (RMSD) plot for the DNA residues during 40 ns for each molecular dynamics simulation; and (C) Interaction between **16** and residues DC21, DG22, DG4, and DC3 of ctDNA through van der Waals interactions, and additional H-bond between DC3 residue and amino groups a length of 2.4 Å.

3. Conclusion

Seven from twenty chromenes possessed high potency throughout the cancer human cell lines tested. In general, the *para*-position electron-withdrawing substituents on the phenyl ring are favored towards potency and selectivity for cancer cells. The nucleic acid interaction studies verified that the evaluated chromenes derivatives interact with the DNA model and lead to the supramolecular complex formation. In the exploratory correlation between the binding constants ($\log K_b$) and GI_{50} values, it was observed that the correlation coefficients were negatives to U251, MCF7, NCI-ADR/RES, 786-0, NCI–H460, and OVCAR-3, suggesting that the possible preferential mechanism of action of these compounds may be associated with DNA as a biological target. Experimental biophysical and theoretical studies have suggested that such chromenes derivatives can interact with DNA preferentially *via* intercalation. Finally, the docking and dynamic molecular studies confirmed the spectroscopic results obtained.

4. Experimental

4.1. Chemistry

4.1.1. General procedures

The reagents were obtained by chemicals suppliers and utilized without further purification. Solvents were purified by simple distillation. The reaction progress was monitored by thin-layer chromatography and by gas chromatography-mass spectrometry (GC-MS) on a Shimadzu CGMS-QP2010 ULTRA. The melting point was performed on a GEHAKA-PF1500 apparatus, and the values were not corrected. The NMR spectrum was obtained on a Bruker AVANCE DPX 200 (200 MHz for ^{1}H, 50 MHz for ^{13}C). The data were reported as follows: chemical shift multiplicities [s (singlet), d (doublet), t (triplet), or m (multiplet)] coupling constants

(Hz), integration. The chemical shifts were reported in parts per million (ppm) relative to tetramethylsilane (TMS) peak for ^{1}H and to residual solvent peak for ^{13}C. The infrared spectra were recorded as KBr plates by infrared Fourier transform spectrometry on a Perkin Elmer FTIR RX1 spectrometer 400-4000 cm^{-1}.

The spectrofluorimetric titrations were carried out in an RF-5301 spectrofluorimeter (Shimadzu, Japan) equipped with a source of Xenon lamp (150 W) using a quartz cuvette with 10 mm of the optical path. UV spectra were recorded in AJX-6100PC double beam spectrophotometer (Micronal S.A., Brazil).

4.1.2. General procedure for the synthesis of chromenes

Chromenes **1-18** were synthesized using the protocol previously reported by our research group [30]. The physical and spectral data for compounds **1-15** and **16-18** are in excellent agreement with those reported respectively in literature [30,31] (see Supplementary Materials). Briefly, to a flask, aldehyde (1.0 mmol), malononitrile (1.1 mmol), ammonium formate (0.2 mmol), and 4 mL of aqueous ethanol (1:1) were added to a reaction flask. The mixture was magnetically stirred for 20 min at room temperature, then dimedone (**I**-series) or 4-hydroxycoumarin (**II**-series) or α-naphthol (**III**-series) (1.1 mmol) was added to the mixture and stirred at room temperature for 2 h in cases of **I**- and **II**-series but refluxed for 3 h in case of **III**-series to complete the conversion. The precipitate formed during the reaction was filtered, washed with cold aqueous ethanol to obtain the crude product. Chromenes **1-18** were purified by recrystallization from aqueous ethanol.

4.1.3. General procedure to compounds 19 and 20

To a solution of the respective nitro compound (250 mg, 0.725 mmol) in ethanol (50 mL) were added hydrazine hydrate (1.5 mL, 80% solution in water) and a catalytic amount of 10% palladium on activated charcoal. The reaction was kept under magnetic stirring at 80 °C for 20 min. After

this period, the catalyst was removed by filtration in celite, and the filtrate was evaporated under reduced pressure. To the residue were added 30 mL of dichloromethane and 30 mL of water. The organic layer was extracted and dried over anhydrous magnesium sulfate. After removing the solvent, the crude product was obtained as a solid in 99% yield.

2-Amino-4-(4-aminophenyl)-4H-benzo[h]chromene-3-carbonitrile (19): Mp: 217.5-218.2 °C. IR (KBr, cm^{-1}): 3476, 3452, 3388, 3326, 3192, 3052, 3014, 2878, 2372, 2194, 1652, 1634, 1604, 1574, 1514, 1400, 1374, 1290, 1262, 1184, 1176, 1100, 1020, 792, 768, 746. ^{1}H NMR (200 MHz, DMSO-d_6): 8.24 (d, J = 7.9 Hz, 1H), 7.88 (d, J = 7.6 Hz, 1H), 7.71-7.46 (m, 3H), 7.23-7.01 (m, 3H), 6.91 (d, J = 8.1 Hz, 2H), 6.52 (d, J = 8.1 Hz, 2H), 5,02 (s, 2H); 4,69 (s, 1H). ^{13}C NMR (50 MHz, DMSO-d_6): 159.9, 147.5, 142.5, 133.0, 132.5, 128.2, 127.6, 126.5, 126.4, 123.6, 122.8, 120.7, 120.6, 118.8, 114.0, 57.1, 40.2. HRMS (ESI, IT-TOF) calculated for $C_{20}H_{16}N_3O^+$: 314.1288 Da; found: m/z 314.1294.

2-Amino-4-(3-aminophenyl)-4H-benzo[h]chromene-3-carbonitrile (20): Mp: 132.2-134.7 °C. IR (KBr, cm^{-1}): 3452, 3386, 3324, 3052, 3014, 2876, 2366, 2194, 1654, 1632, 1604, 1574, 1514, 1400, 1374, 1290, 1262, 1176, 1100, 1020, 792, 768, 562. ^{1}H NMR (200 MHz, DMSO-d_6): 8.24 (d, J = 7.9 Hz, 1H), 7.89 (d, J = 7.5 Hz, 1H), 7.72-7.46 (m, 3H), 7.18-7.03 (m, 3H), 6.95 (t, J = 7.5 Hz, 1H), 6.53-6.34 (m, 3H), 5.05 (s, 2H), 4.68 (s, 1H). ^{13}C NMR (50 MHz, DMSO-d_6): 160.0, 149.0, 146.4, 142.6, 132.6, 129.0, 127.6, 126.6, 126.5, 126.3, 123.7, 122.8, 120.6, 118.2, 115.3, 112.9, 112.7, 56.6, 41.2. HRMS (ESI, IT-TOF) calculated for $C_{20}H_{16}N_3O^+$: 314.1288; found: m/z 314.1285.

4.1.4. Single crystal structure determination

The selected single crystal of compounds **19** and **20** were mounted and aligned on a κ-goniostat before exposition to graphite-monochromated X-ray beam from Mo (Kα, λ = 0.71073 Å). An Enraf-Nonius Kappa-CCD diffractometer equipped with a CCD camera was used in the room temperature X-ray diffraction data collect upon φ and ω scans and κ offsets. The crystallographic softwares were used as follows: COLLECT (X-ray diffraction experiment monitoring) [63], HKL Denzo-Scalepack package of softwares (indexing, integration, and scaling of raw data) [64], SIR2004 (structure solving) [65], SHELXL-2018 (structure refinement) [66], and ORTEP (structure analysis and graphical representations) [32]. The structure was solved using the direct methods of phase retrieval wherein all non-hydrogen atoms were directly located from the Fourier synthesis map. The early solved model was refined by the full-matrix least-squares method based on F2 with free anisotropic and fixed isotropic atomic displacement parameters for non-hydrogen and hydrogen atoms. The isotropic atomic displacement parameters of hydrogens were 20% greater than the equivalent isotropic parameter of the bonded atom. Concerning the positions of hydrogens, bond distances were stereochemically constrained according to the riding model with lengths of 0.93 Å (C_{sp}^2—H), 0.98 Å (C_{sp}^3—H), or 0.86 Å (N–H, even though the positions of these hydrogens were first correctly identified in the difference Fourier map before constraining them).

4.2. Biological activities

4.2.1. Antiproliferative assay

Human tumor U251 (glioma), MCF-7 (breast), NCI-ADR/RES (adriamycin-resistant ovarian), 786-0 (kidney), NCI–H460 (lung, non-small cells), PC-3 (prostate), OVCAR-3 (ovarian adenocarcinoma), K-562 (chronic myelogenous leukemia) cell lines as well as the standard HaCaT (keratinocyte) line were kindly provided by the Frederick Cancer Research & Development Center, National Cancer Institute, Frederick, MA, USA. Stock cultures were grown in RPMI 1640 (Gibco BRL, Life Technologies) supplemented with 5% of fetal bovine serum (FBS), penicillin (final concentration 1 mg mL^{-1}), and streptomycin (final concentration 200 U mL^{-1}) [67–69]. Cells were plated in 96-well plates (100 μL cells/well) and exposed to compounds **1**-**20** (0.25–250 μg mL^{-1}) for 48 h at 37 °C in an atmosphere of 5% CO$_2$. Then, the cells were fixed

with 50% trichloroacetic acid and subjected to a sulforhodamine B assay for cell proliferation quantitation at 540 nm [70]. The GI$_{50}$ values of the compounds were determined using a non-linear regression analysis using the Origin 7.5 software (OriginLab Corporation). Doxorubicin (DOX) was used as a reference drug, and the results presented are from two independent experiments, each performed in triplicate.

4.3. Biophysical of ctDNA interaction with chromene derivatives

4.3.1. Reagents and solutions

To prepare the ctDNA solution (*Calf thymus*, Sigma), was weighed between 1 and 2 mg of nucleic acid and solubilized in 2.0 mL of Tris-HCl buffer (10 mM, pH = 7.20 ± 0.10), under stirring for 24 h, and then, the stock solution was stored at 4 °C. Using UV–vis was determined the concentration of the ctDNA in the stock solution at 260 nm (ε_{260} = 6600 M^{-1} cm^{-1} at 25 °C) [71]. The DNA purity was assessed based on the absorbance ratio at 260 and 280 nm, and the value obtained between 1.8 and 2.0 indicates the purity of nucleic acid (protein-free) [72]. The evaluated chromene derivatives (**13-20**) were prepared by weighing 1.0 mg of the compounds and solubilizing them in DMSO; the subsequent dilutions were performed in Tris-HCl buffer. Other reagents used in the assays were of analytical grade with a purity minimum of 98%. Ultrapure water (18.2 MΩ cm^{-1}) was used in all the experiments to prepare the solutions (Gehaka, Brazil).

4.3.2. Procedures

In the spectrofluorimetric titration studies, the chromenes' concentration was kept constant (10 μM) and increasing amounts of ctDNA were added (10–400 μM). The UV–Vis spectroscopy assays measured the spectra of free compounds (10 μM), binding to the ctDNA (100 μM) and free macromolecules. When necessary, a mathematical correction of the signals was performed to correct the internal filter effect [38]. Also, a stock solution of KI 0.2 M was used to evaluate the competitive binding mode, while methylene blue (MB) was 50 μM. Fluorescence measurements with MB were performed in synchronized mode, with Δλ = 40 nm.

4.4. Theoretical studies of ctDNA interaction with chromene derivatives

The dodecamer structure was taken from Protein Data Bank (PDB entry: 1BNA) [73]. The simulated compounds **13-18** were constructed and optimized using the Marvin® software and the Dock prep module of the USCF Chimera® program [74,75]. A blind docking was performed using Autodock Vina® [76] to identify a potential active site in the DNA structure. After the docking procedure, the lower energy conformation for each molecule was chosen as the initial conformation for the molecular dynamics (MD) simulations. The MD was performed using GROMACS® MD package [77]. The PARMBSC1 force field was applied to the DNA. The GROMOS 54A7 force field was added to the ligands using Automated Topology Builder (ATB) and Repository Version 3.0 [78]. In the first stage, the ligands and DNA structure were fixed in a 1.0-nm box octahedron, and water molecules and ions at 0.15 M were added to the system were minimized by the 10,000 steps by the conjugate gradient method. In the second step, the entire system was minimized by 20.000 steps. Then, a slow constant volume heating (NVT) up to 300 K in 1 ns was performed with a time interval of 2 fs. The system density was equilibrated under constant pressure and temperature (NPT) conditions during 1 ns. Finally, the simulation was performed at 40 ns. The MD analysis module of the UCSF Chimera was used to group the most important and predominant conformations into the system. The pose interactions of each ligand in the simulations were visualized by UCSF Chimera and VMD softwares [79]. All RMSD charts were generated by Xmgrace® software [80].

Appendix A. Supplementary data

Supplementary data to this article can be found online at https://doi.org/10.1016/j.ejmcr.2022.100030.

References

[1] R. Pratap, V.J. Ram, Natural and synthetic chromenes, fused chromenes, and versatility of dihydrobenzo[h]chromenes in organic synthesis, Chem. Rev. 114 (2014) 10476–10526, https://doi.org/10.1021/cr500075s.

[2] K.S. Masters, S. Bräse, Xanthones from fungi, lichens, and bacteria: the natural products and their synthesis, Chem. Rev. 112 (2012) 3717–3776, https://doi.org/10.1021/cr100446h.

[3] P. Gebhardt, K. Dornberger, F.A. Gollmick, U. Gräfe, A. Härtl, H. Görls, B. Schlegel, C. Hertweck, Quercinol, an anti-inflammatory chromene from the wood-rotting fungus Daedalea quercina (Oak Mazegill), Bioorg. Med. Chem. Lett 17 (2007) 2558–2560, https://doi.org/10.1016/j.bmcl.2007.02.008.

[4] K.H. Jang, B.H. Lee, B.W. Choi, H.S. Lee, J. Shin, Chromenes from the brown alga Sargassum siliquastrum, J. Nat. Prod. 68 (2005) 716–723, https://doi.org/10.1021/np058003i.

[5] B.P. Moore, Coumarin-like substances from Australian termites, Nature 195 (1962) 1101–1102, https://doi.org/10.1038/1951101a0.

[6] M. Nikpassand, L. Fekri, H. Badri, L. Asadpour, Synthesis and antimicrobial activity of Mono, Bis and Tris 2-amino-4HChromenes, Lett. Org. Chem. 12 (2015) 685–692, https://doi.org/10.2174/1570178612101511102151656.

[7] N.K. Rao, T.N. Rao, B. Parvatamma, K.P. Devi, S.C. Setty, Multi component one pot synthesis and characterization of derivatives of 2-amino-7,7-dimethyl-5-oxo-4-phenyl-5,6,7,8-tetrahydro-4H-chromene-3-carbonitrile and study of antimicrobial activity, Bull. Chem. Soc. Ethiop. 32 (2018) 133–138, https://doi.org/10.4314/bcse.v32i1.12.

[8] F. Crops, M.A. Stahmann, C.F. Huebner, K.P. Link, Studies ON the hemorrhagic sweet clover disease: V. Identification and synthesis OF the hemorrhagic agent, J. Biol. Chem. 138 (1941) 513–527. http://www.jbc.org/content/138/2/513.short.

[9] V. Bhaskar, R. Chowdary, S.R. Dixit, S.D. Joshi, Synthesis, molecular modeling and BACE-1 inhibitory study of tetrahydrobenzo[b] pyran derivatives, Bioorg. Chem. 84 (2019) 202–210, https://doi.org/10.1016/j.bioorg.2018.11.023.

[10] J.M. Batista, A.A. Lopes, D.L. Ambrósio, L.O. Regasini, M.J. Kato, V.D.S. Bolzani, R.M.B. Cicarelli, M. Furlan, Natural chromenes and chromene derivatives as potential anti-trypanosomal agents, Biol. Pharm. Bull. 31 (2008) 538–540, https://doi.org/10.1248/bpb.31.538.

[11] K.V. Sashidhara, J.N. Rosaiah, G. Bhatia, J.K. Saxena, Novel keto-enamine Schiffs bases from 7-hydroxy-4-methyl-2-oxo-2H-benzo[h] chromene-8,10-dicarbaldehyde as potential antidyslipidemic and antioxidant agents, Eur. J. Med. Chem. 43 (2008) 2592–2596, https://doi.org/10.1016/j.ejmech.2007.10.029.

[12] Y. Wang, S.-X. Huang, P. Xia, Y. Xia, Z.-Y. Yang, N. Kilgore, S.L. Morris-Natschke, K.-H. Lee, Anti-AIDS agents 72. Bioisosteres (7-carbon-DCKs) of the potent anti-HIV lead DCK, Bioorg. Med. Chem. Lett 17 (2007) 4316–4319, https://doi.org/10.1016/j.bmcl.2007.05.026.

[13] N.E. Vergel, J.L. López, F. Orallo, D. Viña, D.M. Buitrago, E. del Olmo, J.A. Mico, M.F. Guerrero, Antidepressant-like profile and MAO-A inhibitory activity of 4-propyl-2H-benzo[h]-chromen-2-one, Life Sci. 86 (2010) 819–824, https://doi.org/10.1016/j.lfs.2010.04.001.

[14] S.A. Patil, J. Wang, X.S. Li, J. Chen, T.S. Jones, A. Hosni-Ahmed, R. Patil, W.L. Seibel, W. Li, D.D. Miller, New substituted 4H-chromenes as anticancer agents, Bioorg. Med. Chem. Lett 22 (2012) 4458–4461, https://doi.org/10.1016/j.bmcl.2012.04.074.

[15] A.M. Shestopalov, Y.M. Litvinov, L.A. Rodinovskaya, O.R. Malyshev, M.N. Semenova, V.V. Semenov, Polyalkoxy substituted 4H-chromenes: synthesis by domino reaction and anticancer activity, ACS Comb. Sci. 14 (2012) 484–490, https://doi.org/10.1021/co300062e.

[16] W. Kemnitzer, J. Drewe, S. Jiang, H. Zhang, Y. Wang, J. Zhao, S. Jia, J. Herich, D. Labreque, R. Storer, K. Meerovitch, D. Bouffard, R. Rej, R. Denis, C. Blais, S. Lamothe, G. Attardo, B. Tseng, S. Kasibhatla, S.X. Cai, Discovery of 4-aryl-4 H -chromenes as a new series of apoptosis inducers using a cell- and caspase-based high-throughput screening assay. 1. Structure−Activity relationships of the 4-aryl group, J. Med. Chem. 47 (2004) 6299–6310, https://doi.org/10.1021/jm049640t.

[17] S.X. Cai, J. Drewe, W. Kemnitzer, Discovery of 4-aryl-4H-chromenes as potent apoptosis inducers using a cell- and caspase-based anti-cancer screening apoptosis program (ASAP): SAR studies and the identification of novel vascular disrupting agents, Anti Cancer Agents Med. Chem. 9 (2009) 437–456, https://doi.org/10.2174/1871520610909040437.

[18] S.A. Patil, R. Patil, L.M. Pfeffer, D.D. Miller, Chromenes: potential new chemotherapeutic agents for cancer, Future Med. Chem. 5 (2013) 1647–1660, https://doi.org/10.4155/fmc.13.126.

[19] D.L. Wood, D. Panda, T.R. Wiernicki, L. Wilson, M.A. Jordan, J.P. Singh, Inhibition of mitosis and microtubule function through direct tubulin binding by a novel antiproliferative naphthopyran LY290181, Mol. Pharmacol. 52 (1997) 437–444, https://doi.org/10.1124/mol.52.3.437.

[20] D. Kumar, P. Sharma, H. Singh, K. Nepali, G.K. Gupta, S.K. Jain, F. Ntie-Kang, The value of pyrans as anticancer scaffolds in medicinal chemistry, RSC Adv. 7 (2017) 36977–36999, https://doi.org/10.1039/c7ra05441f.

[21] A. Kumar, V. Jaitak, Natural products as multidrug resistance modulators in cancer, Eur. J. Med. Chem. 176 (2019) 268–291, https://doi.org/10.1016/j.ejmech.2019.05.027.

[22] F. Bray, J. Ferlay, I. Soerjomataram, R.L. Siegel, L.A. Torre, A. Jemal, Global cancer statistics 2018: GLOBOCAN estimates of incidence and mortality worldwide for 36 cancers in 185 countries, CA, Cancer J. Clin. 68 (2018) 394–424, https://doi.org/10.3322/caac.21492.

[23] M.F. Brana, M. Cacho, A. Gradillas, B. de Pascual-Teresa, A. Ramos, Intercalators as anticancer drugs, Curr. Pharmaceut. Des. 7 (2005) 1745–1780, https://doi.org/10.2174/1381612013397113.

[24] C. Avendano, J.C. Menendez, Medicinal Chemistry of Anticancer Drugs, second ed., Elsevier Science, 2015. https://books.google.com.br/books?id=VEiBwAAQBAJ.

[25] D. Agudelo, P. Bourassa, G. Bérubé, H.A.A. Tajmir-Riahi, Review on the binding of anticancer drug doxorubicin with DNA and tRNA: structural models and antitumor activity, J. Photochem. Photobiol. B Biol. 158 (2016) 274–279, https://doi.org/10.1016/j.jphotobiol.2016.02.032.

[26] W.E. Ross, M.O. Bradley, DNA double-strand breaks in mammalian cells after exposure to intercalating agents, BBA Sect. Nucleic Acids Protein Synth. 654 (1981) 129–134, https://doi.org/10.1016/0005-2787(81)90145-3.

[27] M. D'Incalci, C. Sessa, DNA minor groove binding ligands: a new class of anticancer agents, Expet Opin. Invest. Drugs 6 (1997) 875–884, https://doi.org/10.1517/13543784.6.7.875.

[28] V.S. Sibirtsev, A.V. Garabadzhiu, Spectral study of the interaction of DNA with benzothiazolyl-benz-α- chromene, Biochem 72 (2007) 901–909, https://doi.org/10.1134/S0006297907080123.

[29] M.F. Dehkordi, G. Dehghan, M. Mahdavi, M.A.H. Feizi, DNA binding study of dihydropyrano [3, 4-C] chromene derivative by some spectroscopic Techniques, J. Rep. Pharm. Sci. 5 (2016) 80–88.

[30] G. Brahmachari, S. Laskar, B. Banerjee, Eco-friendly, one-pot Multicomponent synthesis of pyran annulated heterocyclic scaffolds at room temperature using ammonium or sodium formate as non-toxic catalyst, J. Heterocycl. Chem. 51 (2014) E303–E308, https://doi.org/10.1002/jhet.1974.

[31] S. Balalaie, S. Ramezanpour, M. Bararjanian, J.H. Gross, DABCO-catalyzed efficient synthesis of naphthopyran derivatives via one-pot three-component condensation reaction at room temperature, Synth. Commun. 38 (2008) 1078–1089, https://doi.org/10.1080/00397910701862865.

[32] L.J. Farrugia, WinGX and ORTEP for windows : an update, J. Appl. Crystallogr. 45 (2012) 849–854, https://doi.org/10.1107/S0021889812029111.

[33] P.Y. Muller, M.N. Milton, The determination and interpretation of the therapeutic index in drug development, Nat. Rev. Drug Discov. 1110 (11) (2012) 751–761, https://doi.org/10.1038/nrd3801, 2012.

[34] M. Parveen, A.M. Malla, Z. Yaseen, A. Ali, M. Alam, Synthesis, characterization, DNA-binding studies and acetylcholinesterase inhibition activity of new 3-formyl chromone derivatives, J. Photochem. Photobiol. B Biol. 130 (2014) 179–187, https://doi.org/10.1016/j.jphotobiol.2013.11.019.

[35] A. Mukherjee, S. Mondal, B. Singh, Spectroscopic, electrochemical and molecular docking study of the binding interaction of a small molecule 5H-naptho[2,1-f][1,2] oxathieaphine 2,2-dioxide with calf thymus DNA, Int. J. Biol. Macromol. 101 (2017) 527–535, https://doi.org/10.1016/j.ijbiomac.2017.03.053.

[36] S.U. Rehman, T. Sarwar, H.M. Ishqi, M.A. Husain, Z. Hasan, M. Tabish, Deciphering the interactions between chlorambucil and calf thymus DNA: a multi-spectroscopic and molecular docking study, Arch. Biochem. Biophys. 566 (2015) 7–14, https://doi.org/10.1016/j.abb.2014.12.013.

[37] Y. Li, Z.-Y. Yang, Z.-C. Liao, Z.-C. Han, Z.-C. Liu, Synthesis, crystal structure, DNA binding properties and antioxidant activities of transition metal complexes with 3-carbaldehyde-chromone semicarbazone, Inorg. Chem. Commun. 13 (2010) 1213–1216, https://doi.org/10.1016/j.inoche.2010.07.005.

[38] J.R. Lakowicz, Principles of Fluorescence Spectroscopy, Springer US, Boston, MA, 2006, https://doi.org/10.1007/978-0-387-46312-4.

[39] Y.-Q.Q. Wang, H.-M.M. Zhang, Exploration of binding of bisphenol A and its analogues with calf thymus DNA by optical spectroscopic and molecular docking methods, J. Photochem. Photobiol. B Biol. 149 (2015) 9–20, https://doi.org/10.1016/j.jphotobiol.2015.04.029.

[40] M.M.V.M.V. Ramana, R. Betkar, A. Nimkar, P. Ranade, B. Mundhe, S. Pardeshi, In vitro DNA binding studies of antiretroviral drug nelfinavir using ethidium bromide as fluorescence probe, J. Photochem. Photobiol. B Biol. 151 (2015) 194–200, https://doi.org/10.1016/j.jphotobiol.2015.08.012.

[41] F. Jalali, G. Rasaee, Electrochemical, spectroscopic, and theoretical studies on the interaction between azathioprine and DNA, Int. J. Biol. Macromol. 81 (2015) 427–434, https://doi.org/10.1016/j.ijbiomac.2015.08.025.

[42] Y.-Z. Zhang, B. Zhou, X.-P. Zhang, P. Huang, C.-H. Li, Y. Liu, Interaction of malachite green with bovine serum albumin: determination of the binding mechanism and binding site by spectroscopic methods, J. Hazard Mater. 163 (2009) 1345–1352, https://doi.org/10.1016/j.jhazmat.2008.07.132.

[43] N. Shahabadi, S.M. Fili, F. Kheirdoosh, Study on the interaction of the drug mesalamine with calf thymus DNA using molecular docking and spectroscopic techniques, J. Photochem. Photobiol. B Biol. 128 (2013) 20–26, https://doi.org/10.1016/j.jphotobiol.2013.08.005.

[44] M.M. Silva, F.C. Savariz, E.F. Silva-Júnior, T.M. de Aquino, M.H. Sarragiotto, J.C.C. Santos, I.M. Figueiredo, Interaction of β-carbolines with DNA: spectroscopic studies, correlation with biological activity and molecular docking, J. Braz. Chem. Soc. 27 (2016) 1558–1568, https://doi.org/10.5935/0103-5053.20160035.

[45] K. Benner, H. Ihmels, S. Kölsch, P.M. Pithan, Targeting abasic site-containing DNA with annelated quinolizinium derivatives: the influence of size, shape and substituents, Org. Biomol. Chem. 12 (2014) 1725–1734, https://doi.org/10.1039/c3ob42140f.

[46] S. Krautwald, C. Nilewski, M. Mori, K. Shiomi, S. Omura, E.M. Carreira, Bioisosteric exchange of C sp 3 -chloro and methyl substituents: synthesis and initial biological studies of atpenin A5 analogues, Angew. Chem. Int. Ed. 55 (2016) 4049–4053, https://doi.org/10.1002/anie.201511672.

[47] J. Wang, Z.Y. Yang, X.Y. Yi, B.D. Wang, DNA-binding properties studies and spectra of a novel fluorescent Zn(II) complex with a new chromone derivative, J. Photochem. Photobiol. Chem. 201 (2009) 183–190, https://doi.org/10.1016/j.jphotochem.2008.10.022.

[48] J.-H.H. Shi, T.-T.T. Liu, M. Jiang, J. Chen, Q. Wang, Characterization of interaction of calf thymus DNA with gefitinib: spectroscopic methods and molecular docking, J. Photochem. Photobiol. B Biol. 147 (2015) 47–55, https://doi.org/10.1016/j.jphotobiol.2015.03.005.

[49] H.-Y. Shen, X.-L. Shao, H. Xu, J. Li, S.-D. Pan, In vitro study of DNA interaction with trichlorobenzenes by spectroscopic and voltammetric techniques, Int. J. Electrochem. Sci. 6 (2011) 532–547. June 9, 2021, www.electrochemsci.org.

[50] N. Bandyopadhyay, P. Basu, G.S. Kumar, B. Guhathakurta, P. Singh, J.P. Naskar, Biophysical studies on the interaction of a novel oxime based palladium(II) complex with DNA and RNA, J. Photochem. Photobiol. B Biol. 173 (2017) 560–570, https://doi.org/10.1016/j.jphotobiol.2017.06.044.

[51] N. Shahabadi, S. Amiri, Spectroscopic and computational studies on the interaction of DNA with pregabalin drug, Spectrochim. Acta Part A Mol. Biomol. Spectrosc. 138 (2015) 840–845, https://doi.org/10.1016/j.saa.2014.10.104.

[52] M.M. Silva, E.O.O. Nascimento, E.F. Silva, J.X. de Araújo, J.C.C. Santos, I.M. Figueiredo, J.X. de Araújo, C.C. Santana, L.A.M. Grillo, R.S. de Oliveira, C.D. Buarque, P. Costa, Interaction between bioactive compound 11a-N-tosyl-5-deoxi-pterocarpan (LQB-223) and Calf thymus DNA: spectroscopic approach, electrophoresis and theoretical studies, Int. J. Biol. Macromol. 96 (2017) 223–233, https://doi.org/10.1016/j.ijbiomac.2016.12.044.

[53] S.U. Rehman, T. Sarwar, M.A. Husain, H.M. Ishqi, M. Tabish, Studying non-covalent drug–DNA interactions, Arch. Biochem. Biophys. 576 (2015) 49–60, https://doi.org/10.1016/j.abb.2015.03.024.

[54] F.C. Savariz, M.A. Foglio, A.L.T. Goes Ruiz, W.F. da Costa, M. de Magalhães Silva, J.C.C. Santos, I.M. Figueiredo, E. Meyer, J.E. de Carvalho, M.H. Sarragiotto, Synthesis and antitumor activity of novel 1-substituted phenyl 3-(2-oxo-1,3,4-oxadiazol-5-yl) β-carbolines and their Mannich bases, Bioorg. Med. Chem. 22 (2014) 6867–6875, https://doi.org/10.1016/j.bmc.2014.10.031.

[55] F.A. Qais, K.M.M. Abdullah, M.M. Alam, I. Naseem, I. Ahmad, Interaction of capsaicin with calf thymus DNA: a multi-spectroscopic and molecular modelling study, Int. J. Biol. Macromol. 97 (2017) 392–402, https://doi.org/10.1016/j.ijbiomac.2017.01.022.

[56] S. Nafisi, A.A. Saboury, N. Keramat, J.-F. Neault, H.-A. Tajmir-Riahi, Stability and structural features of DNA intercalation with ethidium bromide, acridine orange and methylene blue, J. Mol. Struct. 827 (2007) 35–43, https://doi.org/10.1016/j.molstruc.2006.05.004.

[57] Z. Hu, C. Tong, Synchronous fluorescence determination of DNA based on the interaction between methylene blue and DNA, Anal. Chim. Acta 587 (2007) 187–193, https://doi.org/10.1016/j.aca.2007.01.050.

[58] M. Ortiz, A. Fragoso, P.J. Ortiz, C.K. O'Sullivan, Elucidation of the mechanism of single-stranded DNA interaction with methylene blue: a spectroscopic approach, J. Photochem. Photobiol. Chem. 218 (2011) 26–32, https://doi.org/10.1016/j.jphotochem.2010.11.020.

[59] C.M. da Silva, M.M. Silva, F.S. Reis, A.L.T.G. Ruiz, J.E. de Carvalho, J.C.C. Santos, I.M. Figueiredo, R.B. Alves, L.V. Modolo, Â. de Fátima, Studies on free radical scavenging, cancer cell antiproliferation, and calf thymus DNA interaction of Schiff bases, J. Photochem. Photobiol. B Biol. 172 (2017) 129–138, https://doi.org/10.1016/j.jphotobiol.2017.05.020.

[60] M. de M. Silva, T.S. Macedo, H.M.P. Teixeira, D.R.M. Moreira, M.B.P. Soares, A.L. Ana, V. de L. Serafim, F.J.B. Mendonça-Júnior, M. do Carmo A de Lima, R.O. de Moura, E.F. da Silva-Júnior, J.X. de Araújo-Júnior, M.D. Maria, E. de O.O. Nascimento, T.M.S. Maciel, T.M. de Aquino, I.M. Figueiredo, J.C.C. Santos, Correlation between DNA/HSA-interactions and antimalarial activity of acridine derivatives: proposing a possible mechanism of action, J. Photochem. Photobiol. B Biol. 189 (2018) 165–175, https://doi.org/10.1016/j.jphotobiol.2018.10.016.

[61] S. Das, C.J. da Silva, M. de M. Silva, M.D. de A. Dantas, Â. de Fátima, A.L.T. Góis Ruiz, C.M. da Silva, J.E. de Carvalho, J.C.C. Santos, I.M. Figueiredo, E.F. da Silva-Júnior, T.M. de Aquino, J.X. de Araújo-Júnior, G. Brahmachari, L.V. Modolo, Highly functionalized piperidines: free radical scavenging, anticancer activity, DNA interaction and correlation with biological activity, J. Adv. Res. 9 (2018) 51–61, https://doi.org/10.1016/j.jare.2017.10.010.

[62] D. Ajloo, M. Sangian, M. Ghadamgahi, M. Evini, A.A. Saboury, Effect of two imidazolium derivatives of ionic liquids on the structure and activity of adenosine deaminase, Int. J. Biol. Macromol. 55 (2013) 47–61, https://doi.org/10.1016/j.ijbiomac.2012.12.042.

[63] Nonius, COLLECT, 1998.

[64] Z. Otwinowski, W. Minor, Macromolecular crystallography, Part A. Vol 276, Methods Enzymol. (1997) 307–326.

[65] M.C. Burla, R. Caliandro, M. Camalli, B. Carrozzini, G.L. Cascarano, L. De Caro, C. Giacovazzo, G. Polidori, R. Spagna, SIR2004: an improved tool for crystal structure determination and refinement, J. Appl. Crystallogr. 38 (2005) 381–388, https://doi.org/10.1107/S002188980403225X.

[66] G.M. Sheldrick, Crystal structure refinement with SHELXL, Acta Crystallogr. Sect. C Struct. Chem. 71 (2015) 3–8, https://doi.org/10.1107/S2053229614024218.

[67] F.P.G. Euzébio, F.J.L. dos Santos, D. Piló-Veloso, A.L.T.G. Ruiz, J.E. de Carvalho, D.L. Ferreira-Alves, Â. de Fátima, Effect of 6α,7β-dihydroxyvouacapan-17β-oic acid and its lactone derivatives on the growth of human cancer cells, Bioorg. Chem. 37 (2009) 96–100, https://doi.org/10.1016/j.bioorg.2009.03.004.

[68] F.P.G. Euzébio, F.J.L. dos Santos, D. Piló-Veloso, A.F.C. Alcântara, A.L.T.G. Ruiz, J.E. De Carvalho, M.A. Foglio, D.L. Ferreira-Alves, Â. De Fátima, Synthesis, antiproliferative activity in cancer cells and theoretical studies of novel 6α,7β-dihydroxyvouacapan-17β-oic acid Mannich base derivatives, Bioorg. Med. Chem. 18 (2010) 8172–8177, https://doi.org/10.1016/j.bmc.2010.10.015.

[69] C. Marquissolo, Â. de Fátima, L.K. Kohn, A.L.T.G. Ruiz, J.E. de Carvalho, R. a Pilli, Asymmetric total synthesis and antiproliferative activity of goniothalamin oxide isomers, Bioorg. Chem. 37 (2009) 52–56, https://doi.org/10.1016/j.bioorg.2008.12.001.

[70] A. Monks, D. Scudiero, P. Skehan, R. Shoemaker, K. Paull, D. Vistica, C. Hose, J. Langley, P. Cronise, A. Vaigro-Wolff, M. Gray-Goodrich, H. Campbell, J. Mayo, M. Boyd, Feasibility of a high-flux anticancer drug screen using a diverse panel of cultured human tumor cell lines, JNCI J. Natl. Cancer Inst. 83 (1991) 757–766, https://doi.org/10.1093/jnci/83.11.757.

[71] N. Shahabadi, S. Hadidi, Spectroscopic studies on the interaction of calf thymus DNA with the drug levetiracetam, Spectrochim. Acta Part A Mol. Biomol. Spectrosc. 96 (2012) 278–283, https://doi.org/10.1016/j.saa.2012.05.045.

[72] Y. Cui, E. Hao, G. Hui, W. Guo, F. Cui, Investigations on the interactions of diclofenac sodium with HSA and ctDNA using molecular modeling and multispectroscopic methods, Spectrochim. Acta Part A Mol. Biomol. Spectrosc. 110 (2013) 92–99, https://doi.org/10.1016/j.saa.2013.01.093.

[73] H.R. Drew, R.M. Wing, T. Takano, C. Broka, S. Tanaka, K. Itakura, R.E. Dickerson, Structure of a B-DNA dodecamer: conformation and dynamics, Proc. Natl. Acad. Sci. U.S.A. 78 (1981) 2179–2183, https://doi.org/10.1073/pnas.78.4.2179.

[74] Marvin. http://www.chemaxon.com, 2018.

[75] E.F. Pettersen, T.D. Goddard, C.C. Huang, G.S. Couch, D.M. Greenblatt, E.C. Meng, T.E. Ferrin, UCSF Chimera - a visualization system for exploratory research and analysis, J. Comput. Chem. 25 (2004) 1605–1612, https://doi.org/10.1002/jcc.20084.

[76] O. Trott, A.J. Olson, AutoDock Vina, Improving the speed and accuracy of docking with a new scoring function, efficient optimization, and multithreading, J. Comput. Chem. 31 (2009), https://doi.org/10.1002/jcc.21334. NA-NA.

[77] S. Pronk, S. Páll, R. Schulz, P. Larsson, P. Bjelkmar, R. Apostolov, M.R. Shirts, J.C. Smith, P.M. Kasson, D. Van Der Spoel, B. Hess, E. Lindahl, Gromacs 4.5: a high-throughput and highly parallel open source molecular simulation toolkit, Bioinformatics 29 (2013) 845–854, https://doi.org/10.1093/bioinformatics/btt055.

[78] A.K. Malde, L. Zuo, M. Breeze, M. Stroet, D. Poger, P.C. Nair, C. Oostenbrink, A.E. Mark, An automated force field Topology Builder (ATB) and repository: version 1.0, J. Chem. Theor. Comput. 7 (2011) 4026–4037, https://doi.org/10.1021/ct200196m.

[79] W. Humphrey, A. Dalke, K. Schulten, VMD: visual molecular dynamics, J. Mol. Graph. 14 (1996) 33–38, https://doi.org/10.1016/0263-7855(96)00018-5.

[80] P.J. Turner, XMGRACE, 2005.